

On the nature of the absorber in IRAS 09104+4109: the X-ray and mid-infrared view

C. Vignali,^{1,2*} E. Piconcelli,³ G. Lanzuisi,^{4,5} A. Feltre,⁶ C. Feruglio,⁷ R. Maiolino,³ F. Fiore,³ J. Fritz,⁸ V. La Parola,⁹ M. Mignoli² and F. Pozzi¹

¹ Dipartimento di Astronomia, Università degli Studi di Bologna, Via Ranzani 1, 40127 Bologna, Italy

² INAF – Osservatorio Astronomico di Bologna, Via Ranzani 1, 40127 Bologna, Italy

³ INAF–Osservatorio Astronomico di Roma, Via di Frascati 33, 00040 Monteporzio Catone, Italy

⁴ INAF–IASF Roma, Via Fosso del Cavaliere 100, 00133 Roma, Italy

⁵ INAF–IASF Bologna, Via Gobetti 101, I-40129 Bologna, Italy

⁶ Dipartimento di Astronomia, Vicolo Osservatorio 3, 35122 Padova, Italy

⁷ Institut de RadioAstronomie Millimétrique, 300 rue de la Piscine, Domaine Universitaire, 38406 Saint Martin d’Heres, France

⁸ Sterrenkundig Observatorium, Universiteit Gent, Krijgslaan 281 S9, B-9000 Gent, Belgium

⁹ INAF–IASF Palermo, Via Ugo La Malfa 153, 90146 Palermo, Italy

Accepted 2011 June 2. Received 2011 May 31; in original form 2011 January 7

ABSTRACT

We present a long (≈ 76 ks) *Chandra* observation of IRAS 09104+4109, a hyper-luminous galaxy, optically classified as a Type 2 AGN hosted in a cD galaxy in a cluster at $z = 0.442$. We also report on the results obtained by fitting its broad-band spectral energy distribution. The Compton-thick nature of this source (which has been often referred to as an ‘archetype’ of Compton-thick Type 2 quasars) was formerly claimed on the basis of its marginal detection in the PDS instrument onboard *BeppoSAX*, being then disputed using *XMM-Newton* data. Both *Chandra* analysis and optical/mid-IR spectral fitting are consistent with the presence of heavy ($\approx 1 - 5 \times 10^{23} \text{ cm}^{-2}$), but not extreme (Compton-thick) obscuration. However, using the mid-IR and the [O III] emission as proxies of the nuclear hard X-ray luminosity suggests the presence of heavier obscuration. The 54-month *Swift* BAT map shows excess hard X-ray emission likely related to a nearby ($z=0.009$) Type 2 AGN, close enough to IRAS 09104+4109 to significantly enhance and contaminate its emission in the early *BeppoSAX* PDS data.

Key words: quasars: general — quasars: individual: IRAS 09104+4109 — galaxies: nuclei — galaxies: active

1 INTRODUCTION

IRAS 09104+4109 (hereafter referred to as I09104) is a hyper-luminous infrared cD galaxy at $z=0.442$ residing in the core of a rich cluster of galaxies (Kleinmann et al. 1988). Its optical spectrum is characterized by the presence of narrow emission lines, although broad Balmer and MgII lines were observed in polarized light (Hines & Wills 1993; Tran, Cohen & Villar-Martin 2000). These remarkable results, based on optical observations, suggested the presence of a powerful quasar hidden in I09104. Subsequent X-ray observations confirmed this ‘picture’. While *BeppoSAX* data below 10 keV were ‘contaminated’ by the intra-cluster emission, the weak signal detected by the PDS instrument in the range ≈ 15 –60 keV (in a 34 ks exposure) was interpreted by Franceschini and collaborators (2000, hereafter F00) as the primary emission of the buried quasar, emerging at very high energies because

of Compton-thick absorption (i.e., above $\approx 10^{24} \text{ cm}^{-2}$; in the case of I09104, the estimated lower limit on the column density was $5 \times 10^{24} \text{ cm}^{-2}$). The detection of a strong iron $K\alpha$ emission line, with equivalent width (EW) of ≈ 1 –2 keV – consistent with a reflection scenario for the quasar emission in the 2–10 keV energy range – further supported the Compton-thick nature of I09104 in F00, and similar conclusions, though reached with limited counting statistics (but much higher spatial resolution), were drawn from a 9.1 ks *Chandra* observation (Iwasawa, Fabian & Etori 2001, hereafter I01).

Doubts on these conclusions were recently cast by Piconcelli et al. (2007, hereafter P07) on the basis of the analysis of a 14 ks *XMM-Newton* observation. In particular, although both a transmission- and a reflection-dominated model provided a good fit to the quasar emission, the iron line EW was lower (≈ 400 eV) than expected in the case of a Compton-thick scenario (EW ≈ 1 –2 keV), but it was higher than model predictions for a few $\times 10^{23} \text{ cm}^{-2}$ obscuration (Ghisellini, Haardt & Matt 1994).

* E-mail: cristian.vignali@unibo.it.

Furthermore, the source bolometric luminosity was well recovered using the 2–10 keV flux obtained in a transmission model (after removal of the significant contribution from the cluster, see P07) and assuming a reasonable X-ray bolometric correction (§4 in P07). According to these authors, the weak detection in the PDS instrument onboard *BeppoSAX* was explained by the presence of a heavily obscured, possibly Compton-thick galaxy (NGC 2782; Zhang et al. 2006) in the large (1.3° FWHM) field of view of the PDS.

To date, the number of “certified” (i.e., secured by good-quality X-ray spectra and, possibly, high-energy detection) Compton-thick Active Galactic Nuclei (AGN) is still limited, being settled around $\approx 40 - 50$ and mostly at low ($\lesssim 0.05$) redshifts (see Comastri 2004 for a review on this topic, and Della Ceca et al. 2008 for an updated list of Compton-thick AGN). Large numbers of Compton-thick AGN candidates at higher redshifts have been recently claimed, but their identification as heavily obscured AGN is often derived from other, indirect arguments [e.g., optical emission-line strength, combined mid-infrared (mid-IR) and optical criteria, stacked X-ray emission; e.g., Alexander et al. 2008, 2011; Fiore et al. 2008, 2009; Lanzuisi et al. 2009; Bauer et al. 2010; Gilli et al. 2010, and references therein; Vignali et al. 2010] than direct, good-quality X-ray spectroscopy.

Clearly, the lack of broad-band X-ray instruments within the same observatory (as in *BeppoSAX*) is currently limiting the detection and spectral characterization of Compton-thick AGN; in this regard, the *Integral*-IBIS (Beckmann et al. 2009) and *Swift* BAT (Tueller et al. 2008) surveys have brought to the detection of additional very local Compton-thick AGN candidates, but their confirmation has always required follow-up observations with *Chandra*, *XMM-Newton* or *Suzaku* (e.g., Ueda et al. 2007; Eguchi et al. 2009; Comastri et al. 2010; Severgnini et al. 2011; Burlon et al. 2011). To overcome this observational problem will necessarily rely on the next-generation hard X-ray imager that will fly on *NuSTAR*.

In this context, it is clear the role of our present investigation to assess the “true” nature of I09104, i.e., whether it is Compton thick or Compton thin. If Compton thick, it would be one of the few AGN of this class beyond the local Universe supported by moderately good-quality X-ray spectroscopy (for other moderate/high-redshift Compton-thick AGN, see Norman et al. 2002; Iwasawa et al. 2005; Comastri et al. 2011; Feruglio et al. 2011; Gilli et al. 2011). We tackle this issue through a multi-wavelength approach consisting of (a) the analysis of a long (≈ 76 ks) and recent (2009) *Chandra* observation of I09104 and (b) the reconstruction of its optical and mid- and far-infrared (far-IR) spectral energy distribution (SED) in terms of stellar plus reprocessed AGN emission, using the code developed by Fritz, Franceschini & Hatziminaoglou (2006, hereafter F06). While (a) will provide further clues on the best-fitting model characterizing the X-ray emission of I09104, (b) will allow us to estimate the geometry and coverage of the obscuring matter as well as its column density, which will be compared to that derived from X-rays.

Finally, we use known correlations found in AGN to estimate the expected intrinsic 2–10 keV emission. In particular, we use the $5.8\mu\text{m}$, $12.3\mu\text{m}$ and $[\text{O III}]5007\text{\AA}$ luminosities as a proxy of the nuclear luminosity following the correlations reported by Lanzuisi et al. (2009) and Gandhi et al. (2009) for the mid-IR, and Mulchaey et al. (1994) and Heckman et al. (2005) for the optical. Furthermore, we also compute the 2–10 keV over $[\text{Ne V}]3426\text{\AA}$ flux ratio to possibly place further constraints on the amount of absorption.

A Λ -cosmology with $H_0=70 \text{ km s}^{-1} \text{ Mpc}^{-1}$, $\Omega_M=0.3$ and $\Omega_\Lambda=0.7$ (Spergel et al. 2003) is adopted.

2 CHANDRA DATA

2.1 X-ray data analysis

I09104 was observed on Jan 6th 2009 for 76.16 ks with the Advanced CCD Imaging Spectrometer (ACIS; Garmire et al. 2003) and the I3 CCD at the aimpoint. The observation (OBS_ID=10445) was carried out in very faint mode. Since the source is in a massive cooling-flow cluster (Fabian & Crawford 1995), showing a significant radial temperature gradient, the background subtraction is highly critical, despite the brightness of I09104. Therefore, to extract spectra, we decided to adopt a strategy similar to that applied by I01 to the previous 9.1 ks *Chandra* observation, dating back to 1999. We extracted the source spectrum from a $1''$ -radius region (large enough to include ≈ 85 –90 per cent of the on-axis *Chandra* ACIS PSF) and the background from the surrounding $1''$ – $2''$ annulus, to possibly account for a significant fraction of the cool-core cluster thermal emission. The source extraction region was chosen from the X-ray image above 2 keV, where the contrast between I09104 and the extended emission is maximized. At softer energies, the source does not appear to be point-like, and its location seems consistent with the bright core of the cluster emission. Because of its superior PSF, using *Chandra* data allows us to better evaluate the contribution due to the thermal emission – whose detailed analysis is beyond the purposes of this work – than in the *XMM-Newton* observation (P07). We note that after background removal, ≈ 700 source counts are available for spectral fitting. The resulting spectrum has been grouped with a minimum of 20 counts per bin to apply the χ^2 statistic and fitted with XSPEC v12.5.0 (Arnaud 1996).

The results obtained from this source spectral extraction has been checked - as reported in the following - using a different strategy, consisting of fitting the background contained in the $1''$ – $2''$ annulus, freezing its spectral parameters to their best-fitting values, and then applying this background model (properly scaled to account for the factor 3 difference in area between source and background) to the source spectral components (see §2.2).

Hereafter, errors are quoted at the 90 per cent confidence level for one interesting parameter (i.e., $\Delta\chi^2 = 2.71$; Avni 1976); all spectral fits include absorption due to the line-of-sight Galactic column density of $N_H = 1.42 \times 10^{20} \text{ cm}^{-2}$ (Kalberla et al. 2005), and Anders & Grevesse (1989) abundances are assumed.

2.2 X-ray spectral fitting

To reproduce the *Chandra* data over the 0.5–7 keV energy range, we have adopted two models, similarly to the fitting strategy applied by P07 to *XMM-Newton* data. The first model (hereafter referred to as “transmission” model) comprises an absorbed power-law component plus an iron emission line. The second model (referred to as “reflection” model) includes a reflection component (PEXRAV in XSPEC) and an iron emission feature. These models are reported as A and B in Table 1, where A2 differs from A1 because the powerlaw photon index is fixed to 1.8, as expected and typically found in case of AGN emission (e.g., Piconcelli et al. 2005, and references therein). Furthermore, both models include a soft component due to the residual (i.e., not totally accounted for by background subtraction) cluster thermal emission. It is also possible that there might be a contribution to soft X-rays from photoionized gas at the inner nucleus, as suggested by I01; this hypothesis would be consistent with the hard-to-soft X-ray flux ratio (≈ 4 per cent) observed in I09104, which is comparable to that typically measured

Table 1. Best-fitting spectral parameters for the *Chandra* spectrum of I09104.

Model (1)	kT (2)	Γ (3)	N_H (4)	$E_{K\alpha}$ (5)	$EW_{K\alpha}$ (6)	χ^2/dof (7)
Source: R=1''; Back: annulus 1''–2''						
A1	$3.74^{+5.73}_{-1.24}$	$0.70^{+0.71}_{-0.40}$	$2.59^{+1.42}_{-1.14}$	6.41 ± 0.06	425^{+164}_{-140}	30.0/39
A2	$4.07^{+9.16}_{-1.58}$	1.8 (fr)	$4.29^{+1.25}_{-0.82}$	6.41 ± 0.06	316^{+210}_{-115}	35.1/40
B	$1.44^{+1.00}_{-0.52}$	1.8 (fr)		6.42 ± 0.06	530^{+182}_{-184}	53.2/40
Source: R=1''; Back: annulus 1''–2'' – Separate source and back fitting						
A1	$3.81^{+4.38}_{-1.20}$	$0.74^{+0.44}_{-0.26}$	$2.81^{+0.61}_{-0.72}$	6.42 ± 0.06	337^{+149}_{-112}	26.4/39
A2	$4.02^{+4.81}_{-1.38}$	1.8 (fr)	$4.49^{+0.73}_{-0.69}$	$6.41^{+0.07}_{-0.05}$	274 ± 118	30.8/40
B	$1.44^{+0.65}_{-0.75}$	1.8 (fr)		6.43 ± 0.06	423^{+136}_{-147}	52.0/40

Notes — The source counts are extracted from a circular region centered on I09104 of radius 1'', and the background from the surrounding annulus of size 1''–2''. The top part of the table refers to the “standard” case where the spectral parameters are obtained by subtracting the background to the source+background spectrum within XSPEC. The bottom part of the table reports the same spectral parameters when a different approach (fit to the background counts and subsequent fit to the source data, once the background components, properly normalized by the source area/background area, are frozen to their best-fitting values) is adopted. (1) X-ray modeling: A1: absorbed power-law model + iron line (transmission model); A2: the same, with Γ frozen to 1.8, as expected for AGN emission; B: reflection + iron line (reflection model), with Γ frozen to 1.8. In both models, a thermal component has been included; (2) temperature of the gas in the cluster (fitted with a MEKAL model within XSPEC); (3) power-law photon index; (4) column density (in units of 10^{23} cm^{-2}); (5) rest-frame energy of the iron $K\alpha$ line (in keV), whose width is fixed to 10 eV; (6) rest-frame equivalent width of the iron line (in eV); (7) $\chi^2/\text{degrees of freedom (dof)}$.

in Sey 2 galaxies (e.g., Matt et al. 2004; Piconcelli et al. 2008, and references therein). However, a detailed analysis of the soft X-ray emission, limited by the low number of counts below 2 keV (≈ 200) and the lack of deep X-ray grating data, is beyond the purposes of this paper, since the main goal of our work consists of a proper characterization of the hard (> 2 keV) emission.

In the upper part of Table 1, we report the X-ray spectral results for both models using a “standard” background subtraction within XSPEC, where the source+background spectrum is extracted from a circular region of radius 1'' centered on the position of I09104, and the background spectrum from a surrounding annulus, as anticipated in §2.1. The lower part of Table 1 reports the same models using a different background subtraction strategy; at first, the background, using its own response matrices, is fitted with a thermal component plus a low-normalization powerlaw component. The best-fitting parameters are then frozen, and the source+background spectrum is fitted using these components (multiplied by a normalization constant fixed to 0.33, i.e., the source/background area ratio) and those ascribed to the nucleus of I09104. As evident from Table 1 and already reported above, there is still need for a thermal component, possibly due to the residuals at soft X-ray energies obtained from the best-fitting of the background spectrum. By using the latter background subtraction procedure, errors on the parameters are typically lower.

Whatever the method adopted to account for background-subtraction is, the transmission model is preferred in terms of quality of the fit (see column (7) in Table 1). In this model, the column density is $N_H \approx (1 - 5) \times 10^{23} \text{ cm}^{-2}$, closely resembling the absorption values found by P07. The iron line, compatible with being neutral or mildly ionized, has an $EW \approx 300 - 400 \text{ eV}$ (in the rest frame of the source), is consistent, within errors, with the value found by P07 (and similarly for the line flux) and with that ob-

tained by I01 using lower exposure *Chandra* data. We note that these large EW values, though not extreme, are slightly higher than expected in the case of fluorescence iron line produced by the obscuring matter (Ghisellini et al. 1994)¹ but appear consistent with previous XMM-Newton and Suzaku observations of Compton-thin Seyfert 2 galaxies (e.g., Guainazzi, Matt & Perola 2005; Fukazawa et al. 2011). Given the large stellar mass estimated via SED fitting (which is described in §4), $M_* \approx 4.8 \times 10^{11} M_\odot$, and the known mass-metallicity relation (Lequeux et al. 1979; Savaglio et al. 2005), we may expect some metal (more specifically, iron) enhancement in I09104, hence an increased strength of the Fe emission line, although it is not straightforward to quantify such effect. For instance, NGC 4388, a local Sey 2 galaxy with a column density comparable to that of I09104, shows a similarly large iron $K\alpha$ EW (Iwasawa et al. 2003; see also Beckmann et al. 2004 and Shirai et al. 2008 for significant EW differences due to continuum variability), although it is not hosted by a massive galaxy. On the other hand, we note that Mrk 231 shows a relatively low EW for the iron $K\alpha$ line, despite being a Compton-thick AGN (Braitto et al. 2004). More convincing hints for a Compton-thin absorption towards I09104 are likely provided by the high-energy constraints (see §3).

The 90 per cent upper limit on the EW for He-like and H-like iron line at 6.7 keV and 6.97 keV is $\approx 85 \text{ eV}$. Although the powerlaw is characterized by an apparently flat photon index, the solution with a more physically acceptable $\Gamma = 1.8$ still provides an adequate fit to the data (see Table 1). The source spectrum, fitted

¹ The predicted EW for the iron line depends on the inclination angle of the torus, although this dependence is not strong given the column density range derived from X-ray spectral fitting of I09104 data.

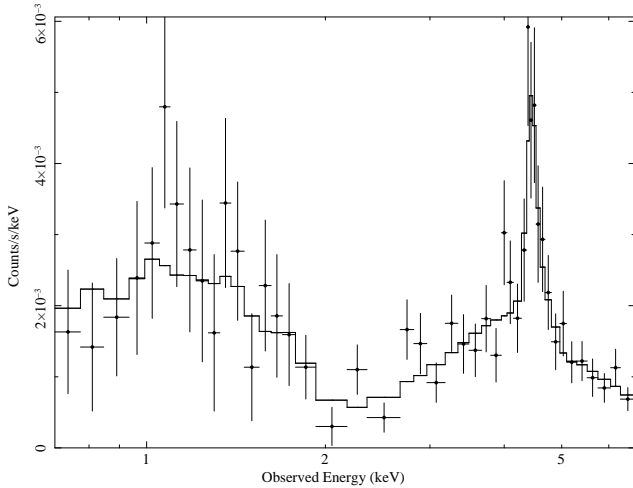


Figure 1. *Chandra* datapoints of I09104 fitted with an absorbed powerlaw plus an iron line (transmission model; A1 model in the top part of Table 1) and thermal emission, ascribed to the cluster.

using a transmission model (including a neutral iron line), is shown in Fig. 1.

The 2–10 keV flux² is $\approx (3.8 - 4.2) \times 10^{-13} \text{ erg cm}^{-2} \text{ s}^{-1}$, corresponding to an intrinsic (i.e., absorption-corrected in the case of models A1/A2) AGN luminosity (placing the contribution due to the residual thermal emission to 0) of $\approx (2.7 - 3.1) \times 10^{44} \text{ erg s}^{-1}$ (where the range of values is ascribed to the differences in the method adopted for background subtraction).

Although the low-energy (below ≈ 6 keV) range provided by *Chandra* is apparently not well suited for placing significant constraints on the reflection component, we modeled the data using a Compton reflection component from neutral matter (PEXRAV model in XSPEC; Magdziar & Zdziarski 1995); we adopted $\cos i = 0.9$ as inclination angle for the reflection component, which is equivalent to assuming a rather face-on geometry for the reflecting material, likely to be associated with the inner walls of the obscuring torus; we chose a cut-off energy of 200 keV for the primary continuum, and metal abundances were fixed to the solar value. We also fixed the photon index of the continuum to 1.8 to facilitate the spectral fitting with the reflection model over the limited energy bandpass provided by *Chandra* and get a reasonable constraint on the strength of such component. The *Chandra* data require a reflection-dominated spectrum, where the primary powerlaw normalization is formally consistent with 0. From a statistical point of view, the reflection model provides a worse description of the X-ray data, regardless of the adopted method to subtract the background (see Table 1). The iron $K\alpha$ emission line EW is $\approx 400 - 500 \text{ eV}$, which is not easily reconcilable with what expected in a typical reflection scenario.

We note that the photon index derived by our spectral fittings in case of a transmission model (A1) is flat. This result can suggest

² Since the currently used version of PSEXTRACT, the tool adopted to extract the X-ray spectrum from *Chandra* data, does not take into account the correction for the encircled energy fraction enclosed in the source extraction region, we compute average “correction factors” to be applied to the fluxes using the *Chandra* Proposer’s Guide. At the on-axis position of our target, these factors, included in the flux and luminosity values reported hereafter, are ≈ 10 and ≈ 18 per cent for the 0.5–2 keV and 2–10 keV bands, respectively.

that an additional reflection component may be present, causing the observed X-ray photon index to be flatter than expected from AGN emission (e.g., Piconcelli et al. 2005); however, a “mixed” absorption and reflection model is not able to provide any improvement to the previous spectral solutions, calling for higher quality data over a possibly more extended energy interval.

Overall, it seems that any residual cluster emission has been taken into account properly by our procedure of background removal and fitting, thanks to the good on-axis PSF provided by *Chandra*. For instance, the ionized iron line components related to extended (cluster) emission may be at the origin of the large iron line EW previously reported (F00).

The *Chandra* data presented in this paper provide consistent results with those published by P07; although the photon statistics is higher in the XMM-Newton observation (which also guarantees data over a broader energy range), *Chandra* data allow us for a better treatment of the contamination from the cluster in virtue of its better PSF. We find that ≈ 90 per cent of the flux is ascribed to the active nucleus over the 2–10 keV range, to be compared with $\approx 30 - 35$ per cent derived by P07, where the source counts were extracted from a much larger $[37'' \text{ (pn)} - 40'' \text{ (MOS)}]$ region.

3 HIGH-ENERGY CONSTRAINTS FROM THE 54-MONTH SWIFT BAT DATA

We used the 54-month *Swift* BAT data, processed using the BAT_IMAGER software (Segreto et al. 2010), to constrain the high-energy emission of I09104. The source is not detected in any of the BAT sub-bands, the 3- σ upper limits to the source X-ray emission (derived using a Crab-like spectrum) being $\approx 1.9 \times 10^{-12}$, $\approx 3.3 \times 10^{-12}$, and $\approx 4.8 \times 10^{-12} \text{ erg cm}^{-2} \text{ s}^{-1}$ in the 15–30 keV, 15–70 keV, and 15–150 keV bands, respectively. The lowest energy upper limit provided by BAT is consistent, within uncertainties, with the flux derived in the 20–30 keV energy range by F00 using *BeppoSAX* data ($\approx 2.5 \times 10^{-12} \text{ erg cm}^{-2} \text{ s}^{-1}$). The flux limit in the BAT map at the position of I09104 (but see below for concerns about possible contamination) is too loose to place any constrain on the two X-ray models presented in §2.2.

As shown in Fig. 2, there is “excess” emission (at the $\approx 4\sigma$ level, i.e., just below the detection threshold adopted for BAT maps) close (at $\approx 17'$) to our source of interest, although such emission, at first glance, appears related to another object. It is reasonable to believe that the upper limit to the hard X-ray emission of I09104 reported above is actually contaminated, at least in part, by the nearby source’s PSF wings and, as such, must be intended as very conservative and poorly indicative of the effective high-energy emission of I09104. This finding provides support to the hypothesis of a Compton-thin absorber towards I09104.

Using the NASA Extragalactic Database (NED) and literature, we have attempted to assign a known counterpart to the source closest to I09104. Taking into account the positional uncertainty in the BAT map ($\approx 6'$, corresponding to the size of the circles in Fig. 2), at the position of the BAT hard X-ray emission we found NGC 2785, a disk galaxy at $z = 0.009$, whose Sloan Digital Sky Survey (SDSS) spectrum is characterized by a very red continuum and a large $H\alpha/H\beta$ ratio (≈ 20.9 at face value, or ≈ 12.5 taking into account the correction for the average host galaxy absorption component), being highly suggestive of a heavily extinguished object. The “corrected” $H\alpha/H\beta$ ratio is consistent with the value reported by Veilleux et al. (1995) using a different optical spectrum. Under reasonable assumptions, this line flux ratio translates into a

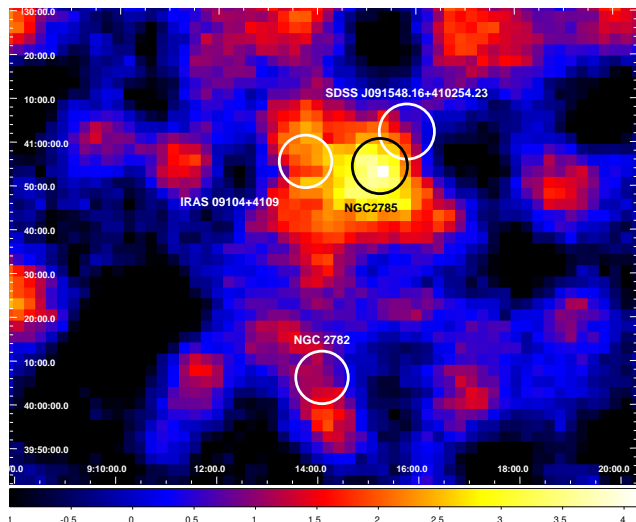


Figure 2. *Swift* BAT 54-month significance map (15–30 keV band) of the area around I09104, clearly showing hard X-ray emission close but likely not associated to the $z = 0.442$ quasar. The position of NGC 2782, previously claimed to contaminate the PDS flux of I09104 (P07), is also shown, along with the positions of NGC 2785 (black circle) and SDSS J091548.16+410254.23; see text for details. All circles have radii of $6'$, broadly corresponding to the positional uncertainty provided by BAT for weak sources. The color scale indicates the intensity level of the pixels in the map.

$E(B-V) \approx 1.5-1.9$. Furthermore, the $H\alpha/[NII]$ and $H\beta/[OIII]$ line ratios are consistent with this source being a Type 2 AGN. The association of the BAT excess with this source appears as the most likely possibility, as also suggested by their good spatial coincidence (see Fig. 2). At present, the only X-ray constraint to the emission of NGC 2785 below 10 keV (over a broader energy range than that allowed by the shallow *ROSAT* All Sky Survey, RASS, where the source is not detected) can be derived by an *ASCA* GIS observation, where the source, located at a large off-axis angle from the nominal pointing, is not detected. Assuming a simple power-law model with $\Gamma=1.8$, the derived 3σ upper limit to its 2–10 keV flux is $\approx 1.2 \times 10^{-13} \text{ erg cm}^{-2} \text{ s}^{-1}$. Using the de-reddened [O III] emission to estimate the intrinsic 2–10 keV flux (adopting the correlation found by Mulchaey et al. 1994), we derive an X-ray flux of $\approx 2.9 \times 10^{-11} \text{ erg cm}^{-2} \text{ s}^{-1}$. At face value, the difference between the upper limit to the hard X-ray flux derived from *ASCA* data and that estimated from the [O III] intensity can be explained assuming an absorber with a column density of at least $\approx 2.6 \times 10^{24} \text{ cm}^{-2}$. However, the upper limits to the X-ray emission of NGC 2785 above 10 keV derived from the BAT instrument are well below the extrapolation of the absorbed powerlaw, thus casting some doubts on either the X-ray flux derived from the [O III] measurement or the adopted model (or both). Pointed and sensitive X-ray observations of NGC 2785 are required to shed light on all these issues.

At a close position, we found another possible (but less likely) optical counterpart, a broad-line SDSS quasar at $z = 2.32$, SDSS J091548.16+410254.23. This quasar has a tentative detection ($\approx 2.4\sigma$) in the RASS at $\approx 19''$. However, from the BAT map, it seems clear that this source does not provide a significant contribution to the observed signal.

Although the association of the high-energy emission with NGC 2785 requires further support, we note that BAT data have clearly shown that contamination in the early PDS data is a valu-

able hypothesis. As a consequence, serious doubts are cast on the Compton-thick nature of I09104, since it was mostly motivated by the admittedly marginal ($\approx 2.5\sigma$) detection in the PDS instrument and the large equivalent width of the iron $K\alpha$ line (F00), which most probably suffered from the contribution of ionized iron features associated to the thermal emission in *BeppoSAX* data.

Furthermore, from the BAT map it seems clear that NGC 2782 ($z = 0.008$), the Seyfert 2 galaxy thought to contaminate the hard X-ray emission of I09104 in the PDS (P07), has marginal emission in the hard X-rays (see Fig. 2), and its distance from the $z = 0.442$ quasar ($\approx 50'$) is beyond any possible contamination in the BAT map.

4 SPECTRAL ENERGY DISTRIBUTION: MULTI-WAVELENGTH DATA AND FITTING

To provide a better understanding of the matter responsible for the X-ray absorption towards I09104, we have investigated the source broad-band properties using the data available in literature. The scientific goal consists of using the reprocessed emission to constrain the physical/geometrical parameters of the absorber (the “postulated” torus in AGN unification schemes) and estimate the bolometric luminosity of the AGN due to accretion of matter onto the black hole. This study requires that all the possible source components emitting in the UV, optical, near-IR, mid-IR, and far-IR bands are properly taken into account in terms of stellar (galaxy) plus nuclear (AGN) components. The broad-band analysis has been carried out by using most of the photometric datapoints available in Table B.4 of Ruiz et al. (2010). In particular, in our SED fitting analysis, we used the XMM-*Newton* Optical Monitor (OM) data (filters UVW2 and UVW1), the SDSS magnitudes (excluding the *i*-band magnitude, given its contamination from strong [O III] emission), the published *Spitzer* IRAC data at $3.6\mu\text{m}$ and $5.8\mu\text{m}$, and MIPS data at $24\mu\text{m}$. The source was also detected by *IRAS* at all wavelengths³ up to $60\mu\text{m}$, while at longer wavelengths (*IRAS* at $100\mu\text{m}$, *SCUBA* at $450\mu\text{m}$ and $850\mu\text{m}$), only upper limits are available. We remind the reader of the non-simultaneity for most of the data used in our analysis. This issue, common to most investigations dealing with SED fitting, likely plays a minor role, given the long timescales for variability expected in case of reprocessed emission by dust. We also note that our photometric points include both nuclear (i.e., AGN-related) and galaxy emission, with both components being accounted for by the adopted broad-band SED-fitting procedure, as described in the following. Finally, as *a-posteriori* check, we have verified that the broad-band modeling adopted to reproduce the emission from I09104 is consistent, in the mid-IR, with the *Spitzer* IRS spectrum available in literature (discussed in §4.1).

Data have been modeled using the code developed by F06, which assumes that the dust, responsible for the reprocessing of the nuclear radiation, consists of graphite and silicate grains distributed in a “flared disc”, “smooth” geometry. Recent high-resolution, interferometric mid-IR observations of nearby AGN (e.g., Jaffe et al. 2004; Tristram et al. 2007; Meisenheimer et al. 2007; Tristram & Schartmann 2011) have confirmed the presence of a geometrically thick, torus-like dust distribution on pc-scales; however, data strongly suggest that this torus is irregular or “clumpy”.

³ For the flux densities at the *IRAS* wavelengths, we refer to the association of I09104 with the *IRAS* Faint Source Catalog object F09105+4108.

Table 2. Best-fitting SED parameters using a “smooth” torus model.

θ	$\tau_{9.7\mu\text{m}}$	Cov. Angle	$E(B-V)$	MF
(1)	(2)	(3)	(4)	(5)
0	3.0	140	0.16	4.9

Notes — For a full description of the parameters, see Fritz et al. (2006). (1) Angle between the line of sight and the equatorial plane of the torus (in degrees); (2) optical depth at $9.7\mu\text{m}$; (3) full covering angle of the torus (in degrees); (4) $E(B-V)$ of the stellar component; (5) “merit function” (sort of χ^2), used to evaluate the goodness of the fit (see text for details).

X-ray variability on short time-scales provides further support to such clumpy-absorption scenario (Risaliti et al. 2007, 2010). In this regard, many codes have been developed over the last decade to deal with clumpy dust distributions (e.g., Nenkova, Ivezić & Elitzur 2002; Nenkova et al. 2008a,b, N08a,b hereafter; Schartmann et al. 2008; Hönig & Kishimoto 2010). We note, however, that fitting broad-band SED data, based on sparse photometric datapoints, with either smooth or clumpy model is not supposed to provide significantly different results (see Dullemond & van Bemmell 2005) in terms of derived AGN bolometric luminosity. In the following, we will mainly focus on the best-fitting parameters obtained by adopting the smooth dust distribution (F06); however, a discussion based on the broad-band data fitting using the clumpy code described by N08a,b will also be provided.

The SED fitting is based on a multi-component analysis, which has been adopted often in recent literature for the analysis of obscured AGN (e.g., Vignali et al. 2009; Hatziminaoglou, Fritz & Jarrett 2009; Pozzi et al. 2010). The observed UV to far-IR SED of I09104 has been de-composed in three distinct components: stars, having the bulk of the emission in the optical/near-IR; hot dust, mainly heated by UV/optical emission due to gas accreting onto the supermassive black hole and whose emission peaks somewhere between a few and a few tens of microns; cold dust, principally heated by star formation.

The stellar component has been included using a set of Simple Stellar Population (SSP) spectra of solar metallicity and ages ranging from ≈ 1 Myr to ≈ 7.3 Gyr, which corresponds to the time elapsed between $z=4$ (the redshift assumed for the stars to form) and $z=0.442$ in the adopted cosmology. A common value of extinction is applied to stars of all ages, and a Calzetti et al. (2000) attenuation law has been adopted ($R_V = 4.05$). Assuming a higher redshift for the event of star formation does not provide significantly different results, while a Milky Way extinction curve produces a slightly worse fit than the one reported here (see Table 2).

The AGN emission, dominating in the mid-IR range, comprises a thermal component due to reprocessing of the nuclear AGN emission, a scattering component and a disc component. In particular, we used an extended version of the model grid described by F06.

Given the presence of data above $24\mu\text{m}$, also an emission component coming from colder, diffuse dust, likely heated by star-formation processes, has been included in the fitting procedure, and it is represented by templates of known starburst galaxies (see Vignali et al. 2009 for details).

Similarly to Vignali et al. (2009) - to which we refer for further details on the adopted procedure and its limitations - we evaluate the goodness of the fit using a “merit function”, defined as $MF = \sum_{i=1}^{N_O} \left(\frac{M_i - O_i}{\sigma_i} \right)^2 / N_O$, where N_O is the number of observed datapoints, M_i and O_i are the model and observed flux densities,

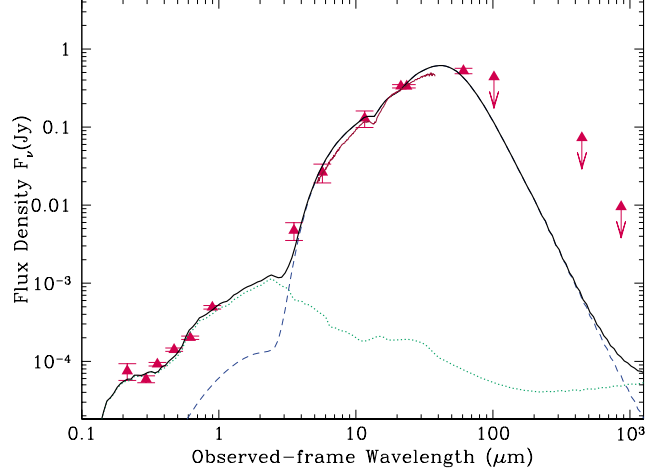


Figure 3. Observed-frame SED of I09104, from the XMM-Newton Optical Monitor (OM) ultraviolet datapoints to the SCUBA $850\mu\text{m}$ datapoint. $3-\sigma$ upper limits refer to non-detections (IRAS $100\mu\text{m}$ and both SCUBA wavelengths). The total SED (thick black line) is the summed contribution of the stellar (green dotted line) and AGN components (blue shaded line). The continuous red line over the wavelength range $\approx 5 - 38\mu\text{m}$ represents the IRS spectrum, without any normalization applied. We note that the best-fitting solution obtained using the F06 model is consistent with the IRS spectrum in terms of normalization and reproduction of the $9.7\mu\text{m}$ silicate absorption feature.

respectively, of the i -th photometric band, and σ_i is the corresponding observed error.

From the SED fitting, there is no need for invoking cold dust ascribed to starburst emission, as suggested by the absence of detected emission in the far-IR above $60\mu\text{m}$ (Fig. 3). The upper limits at longer wavelengths appear fully consistent with AGN emission (see also Rowan-Robinson 2000 for similar conclusions). In the UV/optical band, the stellar component has a moderate extinction [$E(B-V)=0.16$].

The best-fitting solution (Fig. 3) in terms of MF (see Table 2) provides a torus full covering angle of 140° , corresponding to a covering factor of ≈ 90 per cent. The half opening angle, 20° ($[(180-140)/2]$), is larger than the one suggested by the presence of a well collimated radio jet (Kleinmann et al. 1988; Hines & Wills 1993) and a narrow optical ionization cone (Crawford & Vanderriest 1996); see Fig. 3 of Taniguchi et al. (1997). We note, however, that none of the torus models in the grid used in this paper has a covering angle larger than 140° ; to limit the degeneracies in the model parameters, only covering angles of 60, 100, and 140 degrees are actually used (see Fritz et al. 2006). These values refer to three possible “classes” of geometric solutions for the torus: a disk-like torus, a moderate-coverage torus, and one covering most of the nuclear source. Our best-fitting SED delineates a configuration where a significant fraction of the innermost regions of I09104 is hidden by the torus; in these terms, its covering angle can be considered consistent with indications obtained with previous observations.

The extinction at $9.7\mu\text{m}$ along the equatorial plane⁴ is relatively high ($\tau(9.7)=3$) but not extreme, as one might expect in case

⁴ Since the angle between the line of sight and the equatorial plane is zero, the extinction along the line of sight and that along the equatorial plane coincides. Angles different from 0 would imply an extinction in the direction of the observer lower than the equatorial one.

of Compton-thick absorption, and corresponds to a column density of $\approx 1.1 \times 10^{23} \text{ cm}^{-2}$ (assuming a Galactic gas-to-dust ratio conversion). This can be considered broadly consistent with those derived from X-ray spectral analyses [from both *XMM-Newton* (P07) and *Chandra* data; see §2.2]. Given the discrete values for the torus model grid parameters, it is not straightforward to associate uncertainties to the reported values but it is possible to evaluate how much solid the best-fitting solution is. Analysis of the degeneracies in smooth torus parameters (see Pozzi et al. 2010 for details) and corresponding uncertainties indicates that the value of the covering angle of the torus (140°) is well determined, and $\tau(9.7)$ along the equatorial plane reaches at most the value of 6 (90 per cent confidence level), which means a doubling of the column density of the absorber. In all the solutions provided by F06 code for I09104, an absorber with a corresponding column density of at least $\approx 10^{23} \text{ cm}^{-2}$ (but never extreme) is required by the fit.

Overall, the best-fitting solution for the stellar plus nuclear emission of I09104 (Table 2) obtained using, for the reprocessed nuclear component, the smooth dust distribution (F06), is able to reproduce most of the observed photometric datapoints as well as the shape of the IRS spectrum and the $9.7\mu\text{m}$ silicate absorption feature, as discussed in §4.1. The resulting accretion-related bolometric luminosity is $\approx (2.3 - 3.8) \times 10^{47} \text{ erg s}^{-1}$ (where the range provides approximately the 90 per cent uncertainty on the luminosity).

Given the relatively large number of photometric data available and the presence of mid-IR spectroscopic coverage for I09104, this source can be considered a good target for a comparison of smooth vs. clumpy dust distribution; however, for an exhaustive comparison on a large AGN sample, we refer to Feltre et al. (2011). Similarly to the SED fitting described above, we used a stellar plus AGN emission to account for the broad-band emission of I09104. In particular, for the latter component we used the clumpy dust models from N08a,b; according to these models, the dust is distributed in clouds, hence there is always a finite probability for an unobscured (i.e., direct) view of the AGN, irrespective of the viewing angle (e.g., Nikutta, Elitzur & Lacy 2009). Among the latest publicly available grid models (end of September 2010), we adopted those which are considered best suited for Type 2 AGN, where the direct component is likely minor or negligible (R. Nikutta, private communication). This choice is also motivated by the necessity of considering the contribution, at optical and near-IR wavelengths, of the host galaxy stellar component, which is visible in optical images. Including both stellar and direct nuclear components would have provided a over-estimation of the emission at wavelengths short-wards a few microns by the model.

The clumpy model provides a good fit to the observed data in terms of data-to-model residuals ($\text{MF} \approx 4.4$). However, we note two major problems in dealing with this solution (hence, with the parameters derived for the clumpy torus): (a) the model is not able to reproduce the near-IR ($3.6\mu\text{m}$) data, irrespective of the assumed stellar population fitting the optical data. As extensively discussed by Mor, Netzer & Elitzur (2009) and, more recently, by Deo et al. (2011), this emission, not properly accounted for by Nenkova et al. grid models, needs an extra hot-dust component (parameterized by a blackbody with temperature of $\approx 1400 \text{ K}$), possibly associated with graphite grains (which, given a higher sublimation temperature than silicate grains, can survive closer to the black hole; see Mor & Trakhtenbrot 2011). At face value, this result may cast some doubts on the parameters derived in the mid-IR in case of clumpy models. In fact, the extra model component appears hard to justify, since it should be already accounted for by the radiative transfer

treatment, as in smooth torus models. We note, however, that using the Draine & Lee (1984) optical properties for the silicate component (as in Nenkova et al. 2002) instead of the Ossenkopf, Henning & Mathis (OHM; 1992), which have been assumed in N08a,b and recent works (Nikutta et al. 2009), the discrepancy between model and data in the near-IR decreases (see Fig. 4). The second major concern is that (b) the best-fitting clumpy solution to the photometric data is not able to reproduce the shallow $9.7\mu\text{m}$ absorption feature due to silicates in IRS spectrum. This result, which will be discussed further in §4.1, is likely due to the fact that such SED-fitting solution requires the presence of many clouds along the equatorial plane. Their combined contribution manifests itself in a deep silicate feature, which is actually not observed as such in IRS spectrum (see Fig. 4).

Since smooth-torus models are able to account, in a self-consistent way, all of the major components related to direct, scattered and reprocessed AGN emission, we prefer this solution for I09104. However, we caution the reader against over-interpreting our simplistic comparison between the smooth and the clumpy solutions. Extended and more exhaustive checks need to be carried out on a sizable sample of AGN (Feltre et al. 2011) before drawing general conclusions on the capability, by either model, to account for the reprocessed nuclear emission.

For what concerns the smooth torus solution, we note that the SED fitting presented by Taniguchi et al. (1997) suggested the additional presence of cold dust distributed in a much larger outer torus, not included in the radiative transfer modeling. This dust layer would increase the silicate absorption at $9.7 \mu\text{m}$, which has been found to be relatively shallow in IRS data. About the other “inner” torus parameters, their best-fitting solution implies a large covering factor (0.98, not too different from our solution; see discussion in §4) and a larger inclination with respect to the equatorial plane (30°) than ours.

Finally, we may compare the outcome of our SED fitting in terms of gas mass with results from literature. Assuming a typical dust-to-gas mass ratio of 0.01, the dust mass obtained by our SED fitting implies a large gas mass ($\approx 5 \times 10^{10} M_\odot$), a factor $\approx 2 - 3$ higher than the upper limit derived by Evans et al. (1998) through CO measurement. However, both estimates have large uncertainties, mainly related to the underlying assumptions (e.g., significant variations in the dust-to-gas mass ratio across different galaxy populations have been recently reported by Santini et al. 2010).

4.1 IRS spectrum of I09104

Our own analysis of the *Spitzer* IRS spectrum, covering a wavelength range $\approx 5 - 38\mu\text{m}$ in the observed frame, confirms the results reported by Sargsyan et al. (2008; see also Deo et al. 2009); besides the $9.7\mu\text{m}$ silicate feature in absorption, suggestive of obscuration, the IRS spectrum is featureless, except for the very shallow silicate absorption feature, and entirely consistent with the observed mid-IR datapoints (see Fig. 3). The constraints available for the typically most prominent PAH features, not observed in I09104 (see also Sargsyan et al. 2008), are consistent with the lack of a significant starburst component, as found from both the SED fitting analysis (see §4) and using IRAS (Rowan-Robinson 2000) and *ISO* data (Taniguchi et al. 1997). For completeness, we note that in case of a strong radiation field (as in the case of our target), the PAHs can hardly survive, if not properly screened or produced in regions far away from the active nucleus.

We may use the IRS spectrum to make some further considerations about the smooth vs. clumpy solutions for the matter respon-

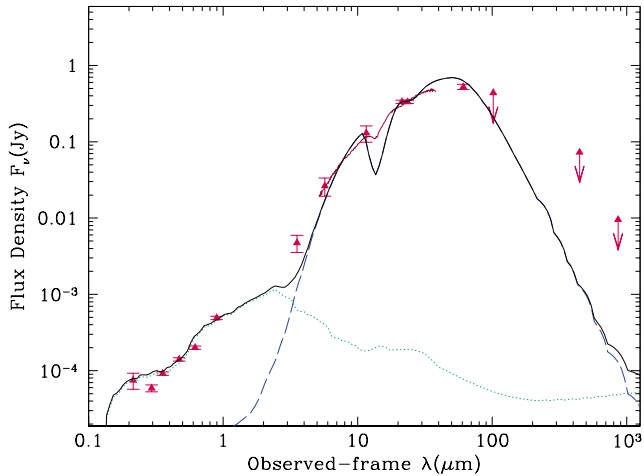


Figure 4. Observed-frame SED of I09104 obtained by fitting the same photometric points as in Fig. 3. The stellar emission (green dotted line) is accounted for using a set of SSPs, while the AGN emission is reproduced using a clumpy dust distribution (blue shaded line). The total SED is marked by the thick black line, while the IRS spectrum is plotted as a continuous red line. The Draine & Lee (1984) optical properties for the silicates have been assumed here (see text for details).

sible for the reprocessing of the nuclear emission in the mid-IR described above. For what concerns the smooth-torus solution, we note that fitting the IRS spectrum alone (without taking into account any stellar component, because of the IRS wavelength coverage) provides, as best-fitting solution, exactly the same found to reproduce the source photometry (see Table 2). Both the shape of the continuum and the $9.7\mu\text{m}$ silicate absorption feature are accounted for reasonably well (see Fig. 3). About the clumpy solution, using the Draine & Lee (1984) optical properties for the silicates produces a good fit to the IRS continuum and $9.7\mu\text{m}$ silicate feature which, on the other side, is never properly reproduced by clumpy models with OHM silicate dust composition. This is opposite to what has recently been reported in literature (e.g., Nikutta et al. 2009). Overall, our results on clumpy tori applied to I09104 indicate that the OHM composition may be rejected, being unable to reproduce the near-IR datapoints and the silicate absorption feature. Clearly, this result, based on a single source, needs to be tested on larger samples. We finally note that in neither case the best-fitting clumpy solution to the IRS spectrum is the same one obtained by fitting the photometric data.

5 DISCUSSION

Two of the evidences that brought F00 towards an interpretation of I09104 as a Compton-thick AGN, i.e., the hard X-ray emission and the large iron $K\alpha$ line EW, have been discussed both by P07 using the XMM-Newton data and in this paper using Chandra data. While the emission above 10 keV detected by the PDS instrument onboard BeppoSAX is very likely associated to a local, obscured AGN (see §3), the large iron emission line EW observed by BeppoSAX was probably originated by a blend of emission features due to the AGN and the cluster. The latter emission has been properly accounted for by the analysis adopted in this paper thanks to the higher Chandra spatial resolution with respect to previous X-ray data which has limited the contamination by extended emission

(see §2.2). The analysis of Chandra data, coupled with the SED results (under the assumption of a smooth dust distribution), suggests that Compton-thin absorption is a likely solution for the absorber close to I09104. However, the upper energy boundary covered with sufficient statistics by Chandra is ≈ 6 keV (observed frame); an extended energy range, possibly coupled with simultaneous data above 10 keV, would be useful to further support this transmission scenario. To provide a broader view of the possible solutions for such absorber, in the following we use known relations to estimate the intrinsic 2–10 keV luminosity of the source (to be compared with the observed luminosity), once the cluster emission has been taken into account. The following relations are characterized by significant dispersions; using them for a single object may suffer from significant limitations, therefore any conclusion drawn in the following should be treated with care.

Given the AGN dominance in the mid-IR, the IRS spectrum of I09104 is used to derive the rest-frame $12.3\mu\text{m}$ flux density and, adopting the Gandhi et al. (2009) correlation (which, obtained from a sample of 42 Seyfert galaxies with near diffraction-limited mid-IR imaging, links the mid-IR luminosity to the 2–10 keV luminosity; see, for a recent application, Vignali et al. 2010), we are able to estimate the expected X-ray emission for this source. On the basis of the SED fitting results (see §4), we do not expect a significant contribution from star formation at these wavelengths.

The predicted AGN 2–10 keV luminosity ($\approx 8.9 \times 10^{45} \text{ erg s}^{-1}$) is higher than the measured value (i.e., not corrected for the absorption) in case of a transmission scenario ($\approx 1.2 - 1.3 \times 10^{44} \text{ erg s}^{-1}$). The predicted/observed luminosity ratio is large and suggestive of Compton-thick obscuration. However, if we use the $5.8\mu\text{m}$ luminosity and the correlation reported in Lanzuisi et al. (2009), which has been obtained for a sample of quasars (i.e., at luminosities comparable to that of I09104), albeit of limited size, we find that the expected 2–10 keV luminosity is $\approx 10^{45} \text{ erg s}^{-1}$, much closer to the observed source luminosity but still suggesting heavy obscuration.

The hard X-ray emission of I09104 can be estimated also using [O III]-based correlations, under the assumption, motivated by unified schemes for AGN, that the [O III]5007Å line is a good proxy of the nuclear emission. Using the value for the [O III] luminosity of I09104 taken from Reyes et al. (2008), not corrected for extinction within the narrow-line region (NLR), we obtain a 2–10 keV luminosity of $5.2 \times 10^{45} \text{ erg s}^{-1}$ and $3.5 \times 10^{45} \text{ erg s}^{-1}$ using the correlation, valid for Type 1 AGN, of Mulchaey et al. (1994) and Heckman et al. (2005), respectively. These values lie in between those obtained from mid-IR estimators and discussed above.

As extensively described in Vignali et al. (2010), these correlations may suffer from the still limited number of objects used to derive them and, in particular, to the small number of AGN at high X-ray luminosity, i.e., in the quasar regime (indicatively above $10^{44} \text{ erg s}^{-1}$, where also I09104 lies). For these reasons, once more we advise against over-interpreting our estimates of the intrinsic nuclear luminosity via the methods reported here, given the overall large uncertainties which characterize these correlations and their application to a single object. However, these results may indicate that some extra absorption with respect to that currently measured by Chandra might be present in I09104.

Finally, we can measure the ratio between the AGN rest-frame 2–10 keV flux prior to absorption correction and the [Ne V] emission line (as available from the SDSS spectrum), and compare the resulting value (≈ 80 –90) to the recent findings published by Gilli et al. (2010). This ratio is expected to decrease for increasing col-

umn density, since the X-ray emission suffers from photo-electric absorption, while the [Ne V] emission, produced in the NLR, can be considered a proxy of the intrinsic nuclear power, although, given its rest-frame wavelength and the fact that it is likely produced in the inner, probably most obscured part of the NLR, it may suffer from extinction. While values above few hundreds are definitively an indication of lack of obscuration, almost all objects with ratios below 15 are Compton thick (see the luminosity plot in Fig. 2 of Gilli et al. 2010 for objects at comparable redshift). Hence, no firm conclusion on the amount of obscuration close to I09104 can be inferred from the X-ray/[Ne V] ratio.

6 SUMMARY

We have presented sensitive *Chandra* data (i.e., with significantly higher photon statistics than those reported by I01) and UV/optical to far-IR SED fitting of the narrow-line quasar I09104 at $z = 0.442$ in order to characterize the properties of the matter responsible for the X-ray absorption and reprocessing of the nuclear radiation in the mid-IR (i.e., the torus envisaged by AGN unification schemes). The source detection in the PDS instrument onboard *BeppoSAX* more than ten years ago has brought I09104 to be classified as a Compton-thick AGN (F00).

In the following, we summarize the main results achieved with the multi-wavelength analysis presented in this work.

- The X-ray spectrum is in favour of a Compton-thin hypothesis, which has also been suggested by P07 from the analysis of XMM-*Newton* data.
- The 54-month *Swift* BAT map in the 15–30 keV energy range has clearly shown that excess hard X-ray emission, if present (since formally below the BAT detection threshold adopted for source catalogs), is likely to be ascribed to NGC 2785, a nearby ($z = 0.009$) Type 2 AGN at $\approx 17'$ from I09104. The properties of its SDSS spectrum are suggestive of heavy extinction.
- Further support to the Compton-thin hypothesis comes from observations at longer wavelengths, where the obscuring matter (torus), responsible for all of the observed emission up to $60\mu\text{m}$, can be well parameterized, providing a $\tau(9.7)=3.0$, consistent with the absorption measured through X-rays (using a Galactic gas-to-dust ratio conversion). The covering factor of the absorber is ≈ 90 per cent. Broad-band photometric data are well reproduced by a stellar component plus a smooth dust distribution (as described by F06); the silicate absorption feature at $9.7\mu\text{m}$ observed in the *Spitzer* IRS spectrum is also properly accounted for by the same torus model. On the other hand, clumpy-torus models (N08a,b), which likely provide a more realistic (physical) description of the obscuring matter (e.g., Tristram et al. 2007), show problems in reproducing the source photometry and spectroscopy at the same time.
- Using the mid-IR (at $12.3\mu\text{m}$ and $5.8\mu\text{m}$, derived directly from the IRS spectrum) and the [O III] emission to predict the hard X-ray luminosity of I09104 provides some space for the presence of additional absorption to be added to the value of column density derived from *Chandra* data.

The scientific case of I09104 strongly supports the importance of broad-band, possibly simultaneous X-ray spectral coverage to define the source complexities properly and provide a robust estimate of the amount of absorption towards the source. In this regard, hard X-ray spectroscopic and imaging capabilities, as those pro-

vided by *NuSTAR* (planned to be launched in 2012), might provide the final answer on the nature of the absorber in I09104.

ACKNOWLEDGMENTS

The authors thanks the referee for his useful comments that improved the quality of the paper, F. Panessa for providing *Spitzer* information about I09104 before publication, and A. Comastri, R. Gilli, R. Nikutta, P. Ranalli, P. Severgnini, D. Vergani, G. Zamorani for insightful suggestions. Partial support from the Italian Space Agency (contracts ASI-INAF I/023/05/0, ASI I/088/06/0, and ASI/INAF/I/009/10/0) is acknowledged. This research has made use of the NASA/IPAC Extragalactic Database (NED) which is operated by the Jet Propulsion Laboratory, California Institute of Technology, under contract with the National Aeronautics and Space Administration, and of data obtained from the Chandra Data Archive and software provided by the Chandra X-ray Center (CXC).

REFERENCES

- Alexander D.M. et al., 2008, *ApJ*, 687, 835
 Alexander D.M. et al., 2011, *ApJ*, 738, 44
 Anders E., Grevesse N., 1989, *Geochim. Cosmochim. Acta*, 53, 197
 Arnaud K.A., 1996, in Jacoby G., Barnes J., eds, *ASP Conf. Ser. Vol. 101, Astronomical Data Analysis Software and Systems V*. Astron. Soc. Pac., San Francisco, p. 17
 Avni Y., 1976, *ApJ*, 210, 642
 Bauer F.E., Yan L., Sajina A., Alexander D.M., 2010, *ApJ*, 710, 212
 Beckmann V., Gehrels N., Favre P., Walter R., Courvoisier T.J.-L., Petrucci P.-O., Malzac J., 2004, *ApJ*, 614, 641
 Beckmann V. et al., 2009, *A&A*, 505, 417
 Braito V. et al., 2004, *A&A*, 420, 79
 Burlon D., Ajello M., Greiner J., Comastri A., Merloni A., Gehrels N., 2011, *ApJ*, 728, 58
 Calzetti D., Armus L., Bohlin R.C., Kinney A.L., Koornneef J., Storchi-Bergmann T., 2000, *ApJ*, 533, 682
 Comastri A., 2004, in “Supermassive Black Holes in the Distant Universe”, ed. A.J. Barger, Kluwer Academic Press, Vol. 308, p. 245
 Comastri A., Iwasawa K., Gilli R., Vignali C., Ranalli P., Matt G., Fiore F., 2010, *ApJ*, 717, 787
 Comastri A., et al., 2011, *A&A*, 526, L9
 Crawford C.S., Vanderriest C., 1996, *MNRAS*, 283, 1003
 Della Ceca R., et al., 2008, *Mem. Soc. Astron. Italiana*, 79, 65
 Deo R.P., Richards G.T., Crenshaw D.M., Kraemer S.B., 2009, *ApJ*, 705, 14
 Deo R.P., Richards G.T., Nikutta R., Elitzur M., Gallagher S.C., Ivezić Ž., Hines D., 2011, *ApJ*, 729, 108
 Draine B.T., Lee H.M., 1984, *ApJ*, 285, 89
 Dullemond C.P., van Bemmell I.M., 2005., *A&A*, 436, 47
 Eguchi S., Ueda Y., Terashima Y., Mushotzky R., Tueller J., 2009, *ApJ*, 696, 1657
 Evans A.S., Sanders D.B., Cutri R.M., Radford S.J.E., Surace J.A., Solomon P.M., Downes D., Kramer C., 1998, *ApJ*, 506, 205
 Fabian A.C., Crawford C.S., 1995, *MNRAS*, 274, L63
 Feltre A., Hatziminaoglou E., Fritz J., Franceschini A., 2011, *MNRAS*, submitted
 Feruglio C., Daddi E., Fiore F., Alexander D.M., Piconcelli E., Malacaria C., 2011, *ApJ*, 729, L4
 Fiore F. et al., 2008, *ApJ*, 672, 94
 Fiore F. et al., 2009, *ApJ*, 693, 447
 Franceschini A., Bassani L., Cappi M., Granato G.L., Malaguti G., Palazzi E., Persic M., 2000, *A&A*, 353, 910 (F00)

- Fritz J., Franceschini A., Hatziminaoglou E., 2006, MNRAS, 366, 767 (F06)
- Fukazawa Y. et al. 2011, ApJ, 727, 19
- Gandhi P., Horst H., Smette A., Hönl S., Comastri A., Gilli R., Vignali C., Duschl W., 2009, A&A, 502, 457
- Garmire G.P., Bautz M.W., Ford P.G., Nousek J.A., Ricker G.R., 2003, Proc. SPIE, 4851, 28
- Ghisellini G., Haardt F., Matt G., 1994, MNRAS, 267, 743
- Gilli R., Vignali C., Mignoli M., Iwasawa K., Comastri A., Zamorani G., 2010, A&A, 519, A92
- Gilli R. et al., 2011, ApJ, 730, L28
- Guainazzi M., Matt G., Perola G.C., 2005, A&A, 444, 119
- Hatziminaoglou E., Fritz J., Jarrett T.H., 2009, MNRAS, 399, 1206
- Heckman T.M., Ptak A., Hornschemeier A., Kauffmann G., 2005, ApJ, 634, 161
- Hines D.C., Wills B.J., 1993, ApJ, 415, 82
- Hönl S.F., Kishimoto M., 2010, A&A, 523, A27
- Iwasawa K., Fabian A.C., Ettori S., 2001, MNRAS, 321, L15 (I01)
- Iwasawa K., Wilson, A.S., Fabian A.C., Young A.J., 2003, MNRAS, 345, 369
- Iwasawa K., Crawford C.S., Fabian A.C., Wilman R.J., 2005, MNRAS, 362, L20
- Jaffe W. et al., 2004, Nature, 429, 47
- Kalberla P.M.W., Burton W.B., Hartmann D., Arnal E.M., Bajaja E., Morras R., Pöppel W.G.L., 2005, A&A, 440, 775
- Kleinmann S.G., Hamilton D., Keel W.C., Wynn-Williams C.G., Eales S.A., Becklin E.E., Kuntz K.D., 1988, ApJ, 328, 161
- Lanzuisi G., Piconcelli E., Fiore F., Feruglio C., Vignali C., Salvato M., Gruppioni C., 2009, A&A, 498, 67
- Lequeux J., Peimbert M., Rayo J.F., Serrano A., Torres-Peimbert S., 1979, A&A, 80, 155
- Magdziarz P., Zdziarski A.A., 1995, MNRAS, 273, 837
- Matt G., Bianchi S., D'Ammando F., Martocchia A., 2004, A&A, 421, 473
- Meisenheimer K., et al., 2007, A&A, 471, 453
- Mor R., Netzer H., Elitzur M., 2009, ApJ, 705, 298
- Mor R., Trakhtenbrot B., 2011, ApJ, 737, L36
- Mulchaey J.S., Koratkar A., Ward M.J., Wilson A.S., Whittle M., Antonucci R.R.J., Kinney A.L., Hurt T., ApJ, 436, 586
- Nenkova M., Ivezić Ž., Elitzur M., 2002, ApJ, 570, L9
- Nenkova M., Sirocky M.M., Ivezić Ž., Elitzur M., 2008a, ApJ, 685, 147 (N08a)
- Nenkova M., Sirocky M.M., Nikutta R., Ivezić Ž., Elitzur M., 2008b, ApJ, 685, 160 (N08b)
- Nikutta R., Elitzur M., Lacy M., 2009, ApJ, 707, 1550
- Norman C., et al., 2002, ApJ, 571, 218
- Ossenkopf V., Henning T., Mathis J.S., 1992, A&A, 261, 567 (OHM)
- Piconcelli E., Jimenez-Bailón E., Guainazzi M., Schartel N., Rodríguez-Pascual P.M., Santos-Lleó M., 2005, A&A, 432, 15
- Piconcelli E., Fiore F., Nicastro F., Mathur S., Brusa M., Comastri A., Puccetti S., 2007, A&A, 473, 85 (P07)
- Piconcelli E., Bianchi S., Miniutti G., Fiore F., Guainazzi M., Jimenez-Bailón E., Matt G., 2008, A&A, 480, 671
- Pozzi F., et al., 2010, A&A, 517, A11
- Reyes R. et al., 2008, AJ, 136, 2373
- Risaliti G., Elvis M., Fabbiano G., Baldi A., Zezas A., Salvati M., 2007, ApJ, 659, L111
- Risaliti G., Elvis M., Bianchi S., Matt G., 2010, MNRAS, 406, L20
- Rowan-Robinson M., 2000, MNRAS, 316, 885
- Ruiz A., Carrera F.J., Panessa F., Miniutti G., 2010, Highlights of Spanish Astrophysics V, Astrophysics and Space Science Proceedings, Diego J.M., Goicoechea L.J., Gonzalez-Serrano J.I. and Gorgas J. eds., Springer-Verlag, 2010, p. 347
- Santini P. et al., 2010, A&A, 518, L154
- Sargsyan L., Mickaelian A., Weedman D., Houck J., 2008, ApJ, 683, 114
- Savaglio S., et al., 2005, ApJ, 635, 260
- Schartmann M., Meisenheimer K., Camenzind M., Wolf S., Tristram K.R.W., Henning T., 2008, A&A, 482, 67
- Segreto A., Cusumano G., Ferrigno C., La Parola V., Mangano V., Mineo T., Romano P., 2010, A&A, 510, A47
- Severgnini P., Caccianiga A., Della Ceca R., Braitto V., Vignali C., La Parola V., Moretti A., 2011, A&A, 525, A38
- Shirai H. et al., 2008, PASJ, 60, 263
- Spergel D.N. et al., 2003, ApJS, 148, 175
- Taniguchi Y., Sato Y., Kawara K., Murayama T., Mouri H., 1997, A&A, 318, L1
- Tran H.D., Cohen M.H., Villar-Martin M., 2000, AJ, 120, 562
- Tristram K.R.W. et al., 2007, A&A, 474, 837
- Tristram K.R.W., Schartmann M., 2011, A&A, 531, A99
- Tueller J., Mushotzky R.F., Barthelmy S., Cannizzo J.K., Gehrels N., Markwardt C.B., Skinner G.K., Winter L.M., 2008, ApJ, 681, 113
- Ueda Y. et al., 2007, ApJ, 664, L79
- Veilleux S., Kim D.-C., Sanders D.B., Mazzarella J.M., Soifer B.T., 1995, ApJS, 98, 171
- Vignali C., et al., 2009, MNRAS, 395, 2189
- Vignali C., Alexander D.M., Gilli R., Pozzi F., 2010, MNRAS, 404, 48
- Zhang J.S., Henkel C., Kadler M., Greenhill L.J., Nagar N., Wilson A.S., Braatz J.A., 2006, A&A, 450, 933